Original Research

Decline of Fiber Tract Integrity Over the Adult Age Range: A Diffusion Spectrum Imaging Study

Stefan J. Teipel, MD,[1,2]* Maximilian Lerche, MD,[1] Ingo Kilimann, MD,[1,2] Kieran O'Brien, PhD,[3] Michel Grothe, PhD,[2] Peter Meyer, MD,[4] Xingfeng Li, PhD,[5] Peter Sänger, PhD,[6] and Karlheinz Hauenstein, MD[6]

Purpose: We applied a novel diffusion spectrum imaging (DSI) acquisition to determine associations between aging and subcortical fiber tract integrity.

Materials and Methods: We studied 35 cognitively healthy subjects (17 women), spanning the adult age range between 23 and 77 years, using anatomical MRI and a novel DSI acquisition scheme at 3 Tesla. The study was approved by the local institutional review board. DSI data were analyzed using tractography and complementary voxel-based analysis of generalized fractional anisotropy (GFA) maps. We determined the effects of age on generalized fractional anisotropy in selected fiber tracts as well as in a whole brain voxel-based analysis. For comparison, we studied the effects of age on regional gray and white matter volumes.

Results: We found a significant reduction in anterior corpus callosum fiber tract integrity with age ($P < 0.001$), as well as significant GFA reduction throughout the subcortical white matter ($P < 0.05$, false discovery rate [FDR] corrected). GFA decline was accompanied by significant gray matter atrophy in frontal and temporal association cortex ($P < 0.05$, FDR corrected).

Conclusion: Our data suggest that normal aging leads to a regionally specific decline in fiber tract integrity. DSI may become a useful biomarker in healthy and pathological aging.

Key Words: white matter microstructure; neurodegeneration; diffusion spectrum imaging; aging; genetics; generalized fractional anisotropy
J. Magn. Reson. Imaging 2014;40:348–359.

NORMAL AGING IS associated with changes in brain structure and function. Predominant decline of prefrontal lobe gray matter (GM) (1) and white matter (WM) (2) volume with normal aging has been described in a range of studies. The underlying mechanism of these alterations is still unresolved. Postmortem autopsy data suggest that cortical thinning with age does not necessarily correspond with a loss of neurons, but may rather be related to changes in neuropil, including dendritic architecture (3), underscoring the role of neuronal connectivity in aging.

Diffusion tensor imaging (DTI) is an MRI technique that measures the directional variability of random water motion. Because water diffusion in the brain is restricted by the direction of fiber tracts, DTI can be used to determine macroscopic architecture (4) and microstructural integrity of white matter (5,6). Consistent with volumetric data, DTI-based measurement of fractional anisotropy (FA), a marker of fiber tract integrity, showed an anterior–posterior gradient of decline with normal aging (7–9), suggesting predominant decline of fiber tract integrity in frontal lobe circuits. Because DTI depends on a Gaussian parameterization of diffusion, it cannot easily resolve crossing and touching fiber bundles which lead to diffusion heterogeneity within an image voxel (10). Diffusion spectrum imaging (DSI) is a model free generalization of DTI that lacks the need to parameterize the diffusion probability and allows reconstruction of crossing fiber tracts with a much higher resolution than conventional DTI (11). To obtain the diffusion spectrum for each voxel, DSI requires a greater coverage of q-space. Therefore, in DSI images not only spatial information is included, but for every voxel multiple points from a cubic lattice in q-space are sampled. The result is that a large number of directions with higher b-values are covered compared

[1]Department of Psychosomatic Medicine, University Medicine Rostock, Rostock, Germany.
[2]DZNE, German Center for Neurodegenerative Diseases, Rostock, Germany.
[3]Centre d'imagerie biomédicale – CIBM, EPFL SB IPSB LIFMET, Lausanne, Switzerland.
[4]Department of Medical Genetics, University Medicine Rostock, Rostock, Germany.
[5]Intelligent Systems Research Centre, University of Ulster, Magee Campus, Derry, BT487JL, Northern Ireland, United Kingdom.
[6]Department of Radiology, University Medicine Rostock, Rostock, Germany.
*Address reprint requests to: S.J.T., University Medicine Rostock, Gehlsheimer Str. 20, 18147 Rostock, Germany. E-mail: stefan.teipel@med.uni-rostock.de
Received April 10, 2013; Accepted July 26, 2013.
DOI 10.1002/jmri.24420
View this article online at wileyonlinelibrary.com.

with DTI. The better coverage of q-space makes DSI inherently more sensitive to the heterogeneity of the diffusion directions within each voxel and with better contrast between fibers of fast or slow diffusion. The improved sensitivity aids the ability of tractography algorithms to resolve all the fibers within a voxel (11). Indeed, DSI studies have shown superior visualization of cingulum bundle integrity (12,13), but so far DSI has not been widely available to study regional and global fiber tract integrity over the adult age range in the human brain due to long acquisition times and specific software requirements.

Of specific interest in the study of human brain aging are the corpus callosum and the cingulum bundle. The corpus callosum provides the main interhemispheric association fiber tract of the human brain and previous DTI studies have shown predominant anterior corpus callosum changes with aging (14). The cingulum bundle is the most prominent fiber tract of the limbic system. It can be divided into a superior component, connecting medial frontal and medial parietal cortices, and an inferior component projecting into parahippocampal white matter. DTI studies suggest that it may be an early indicator for Alzheimer's disease related neurodegeneration in elderly subjects (15,16). In addition to aging, the ApoE4 genotype is an important modulator of brain structure in cognitively unimpaired subjects (17,18) and adds to the risk for sporadic Alzheimer's disease (19).

In the present study we applied a newly developed DSI sequence,to study the effect of aging on white matter microstructural integrity. We used fiber tractography of corpus callosum and cingulate bundle and complementary voxel-based analysis of the generalized fractional anisotropy (GFA) maps (20). Our study served three goals: first, to confirm and extend previous findings from conventional DTI and structural MRI on an anterior to posterior gradient of age related alterations of brain microstructural integrity; second, to test the validity of the newly established DSI sequence; and third, to determine the effect of ApoE4 genotype and cognitive performance on subcortical microstructural integrity.

SUBJECTS AND METHODS

Subjects

We examined 36 subjects (18 women). Data from one female subject (age, 57 years) had to be excluded because of insufficient data quality, leaving 35 subjects (17 women) with a mean age of 50.1 (SD 17.7) years, ranging between 23 and 77 years). The ratio of women to men was 1:1 in each decade between 20–29 and 70–79 years with exception of ages 50–59 where the ratio was 3 men and 2 women.

Global cognitive performance was assessed using the Montreal Cognitive Assessment (MoCA) (21) in subjects 54 years and younger, and the CERAD cognitive battery (22), the Trail Making Test (TMT) parts A and B (23), the Clock Drawing Test (CDT) (24), and the Wechsler Logical Memory test in subjects 55 years and older. All subjects performed within one standard deviation (SD) of the age- and education-adjusted norms in the MOCA and all subtests of the CERAD battery, the TMT-A and B and the Wechsler Logical Memory test, respectively. Mean MOCA score was 28 (SD 1.12) and mean Mini-Mental-Status-Examination (MMSE) score (25) was 28.93 (SD 0.59). CDT score was 1 in all subjects 55 years and older. All subjects scored 0 in the Clinical Dementia Rating (CDR) rating (26). Significant psychiatric comorbidity was ruled out using clinical history and the Patient Health Questionnaire (PHQ-D) (27).

The clinical assessment of subjects included detailed medical history and examination, as well as laboratory tests (complete blood count, electrolytes, glucose, blood urea, creatinine, liver-associated enzymes, total cholesterol, HDL cholesterol, triglycerides, serum B12, folate, thyroid function tests, coagulation status, and serum iron).

The study was approved by the institutional review board. Written informed consent was obtained in every case before examination according to the Declaration of Helsinki.

Neuropsychological Testing

We used the verbal learning and memory test (VLMT) (28), the German version of the auditory verbal learning test (29), as a sensitive measure of learning and episodic memory performance. The VLMT consists of five learning trials of an identical list containing 15 words (DG1 to DG5) followed by an interference list (I). At DG6 the participant is asked to recall the first list again. After a delay of 30 min, participants are once more asked to recall the first list (DG7). For analysis, we used the total learning score (sum of DG1 to DG5), the learning rate (DG5-DG1), the proactive interference (DG1-I) and the retroactive interference (DG5-DG6) (30).

ApoE4 Genotype

Genomic DNA was extracted from a venous blood sample. *APOE* genotyping was conducted according to the standard methods at the Institute of Medical Genetics, University of Rostock using conventional polymerase chain reaction (PCR) with 20 ng of genomic DNA. Primers were designed using Primer 3 online software (http://frodo.wi.mit.edu/) and subsequently checked for biallelic positions using SNPcheck online software (https://ngrl.manchester.ac.uk/SNPCheckV2/snpcheck.htm). The amplification was initiated with denaturation at 95°C for 15 min, amplification by 35 cycles of 94°C for 60 s, 65°C for 60 s, and 72°C for 60 s, and a final extension at 72°C for 6 min. After PCR, the presence of a 533-bp product was confirmed on a 1% agarose gel. PCR products were directly sequenced unidirectionally without prior cleaning procedures using the GenomeLab™ DTCS Quick Start Kit (order number 608120) on a CEQ8800 genetic analysis capillary electrophoresis system (Beckman Coulter GmbH, 47807 Krefeld, Germany).

Image Acquisition

MRI was conducted with a 3.0 Tesla (T) scanner (Magnetom VERIO, Siemens, Erlangen, Germany, maximum gradient 45 mT/m) using a 32-channel head coil. Participants were scanned in a single session without changing their position in the scanner. For anatomical reference, a sagittal high-resolution three-dimensional (3D) gradient echo sequence was performed (magnetization prepared rapid gradient echo (MPRAGE), field-of-view 256 mm, spatial resolution $1.0 \times 1.0 \times 1.0$ mm^3, repetition time 2500 ms, echo time 4.82 ms, inversion time 1100 ms, flip angle 7°, number of slices 180. These data were used for volumetry of gray and white matter and for corpus callosum subregional area measurement. Time of acquisition was 9:20 minutes for this sequence. To identify white matter lesions, a 2D T2-weighted fluid attenuated inversion recovery (FLAIR) sequence was acquired with a repetition time of 9000 ms, an echo time of 94 ms, an inversion time of 2500 ms, 5 mm slice thickness, a distance factor of 20% and 1×0.9 mm in plane resolution, with 24 slices oriented parallel to the anterior to posterior commissure plane. Time of acquisition was 2:24 min for this sequence.

Diffusion spectrum imaging was performed using a twice-refocused 2D-EPI diffusion weighted spin echo sequence (31) (field-of-view 213 mm, Voxel dimension $2.2 \times 2.2 \times 3.0$ mm^3, repetition time 7600 ms, echo time 160 ms, number of slices 38) provided by Siemens Medical Solutions, Erlangen, Germany, WIP #603. One half of q-space was sampled using 257 q-vectors placed on a cubic lattice within a sphere of radius five lattice units and a maximum $b = 7000$ s/mm^2. Acquisition time for the half-scheme acquisition was 33:05 min.

In addition, subjects had undergone a gradient field mapping (time of acquisition 2:11 min) and a resting state fMRI sequence (time of acquisition 11:04 min). These two sequences were obtained for a future combined analysis of functional and structural connectivity, but were not considered in the present study.

Image Processing

Structural MRI Scans (MPRGE Sequence)

The processing of structural MRI scans was implemented through statistical parametric mapping, SPM8 (Wellcome Trust Center for Neuroimaging, London) and the VBM8-toolbox (http://dbm.neuro.uni-jena.de/vbm/) implemented in MATLAB 7.1 (Mathworks, Natwick, MA). First, images were segmented into GM, WM, and cerebrospinal fluid partitions using the tissue prior free segmentation routine of the VBM8-toolbox. The GM and WM partitions of each subject were then high-dimensionally registered to a crisp template of average anatomy in MNI space (IXI-template) using the DARTEL algorithm (32). The IXI-template is part of the VBM8-toolbox and was derived by DARTEL intersubject alignment of 550 healthy control subjects of the publicly available IXI-Database (http://www.brain-development.org).

Flow-fields resulting from the DARTEL registration to the IXI-template were used to warp the GM and WM segments and voxel-values were modulated for nonlinear effects of the high-dimensional normalization. This preserves the total amount of GM and WM volume after linear effects of global head size and shape differences have been accounted for. Finally, modulated warped GM and WM segments were resliced to an isotropic voxel-size of 1.5 mm^3 and smoothed with a Gaussian smoothing kernel of 8 mm full-width at half maximum (FWHM).

Complementary to the voxel-based analysis, we determined the cross-sectional area of the entire corpus callosum in the midsagittal section of the structural MRI scans in native space. Additionally, five subregions in anterior–posterior direction were defined according to the criteria by Hampel et al (33), and segmented using an automated corpus callosum segmentation toolbox implemented in the Automated Registration Toolbox (ART) (Ardekani, BA: yuki module of the Automatic Registration Toolbox (ART) for corpus callosum segmentation, available at http://www.nitrc.org/projects/art). Accuracy of resulting segmentations was visually checked in all scans.

DSI Data

Tractography

Fiber tractography was conducted using DSI-Studio (available at http://dsi-studio.labsolver.org). We used a generalized q-sampling imaging (GQI) reconstruction of the ODF (34). GQI requires the selection of a diffusion sampling length ratio. Empirically, we selected a diffusion sampling length ratio of 1.1 that yielded the most plausible fiber tracts. We used a streamline tracking algorithm with variable fiber lengths and angles as termination criteria depending on the region of interest.

Corpus callosum seed regions for fiber tractography were determined based on a manual segmentation of the cross-sectional corpus callosum area into four segments in anterior to posterior direction (C1 to C4 in Fig. 1). The segmentation was based on equidistant vertical sections through the midsagittal corpus callosum perpendicular to its anterior to posterior length. Fiber tracts were reconstructed separately for each of the four segments with an angle $<60°$ and fiber length between 30 and 100 mm.

Tractography of the cingulum bundle was performed separately for superior and inferior cingulum fibers. For left and right superior cingulum fibers, we placed spherical seed regions in sagittal sections of the generalized fractional anisotropy (GFA) maps superior to the corpus callosum splenium, starting in the first paramedian slice that showed the cingulum bundle and including the next two lateral slices. In addition, we placed a spherical pass region in the coronal view corresponding to the cingulum bundle superior to the middle of the corpus callosum (Fig. 2). Seed regions had a diameter between 10 mm to 12 mm, pass regions between 8 mm and 9 mm, depending on the size of the respective structure in the individual brain scan. Only tracts were allowed with an angle $<30°$ and a fiber length >20 mm. The inferior cingulum fibers were reconstructed in each hemisphere using a spherical

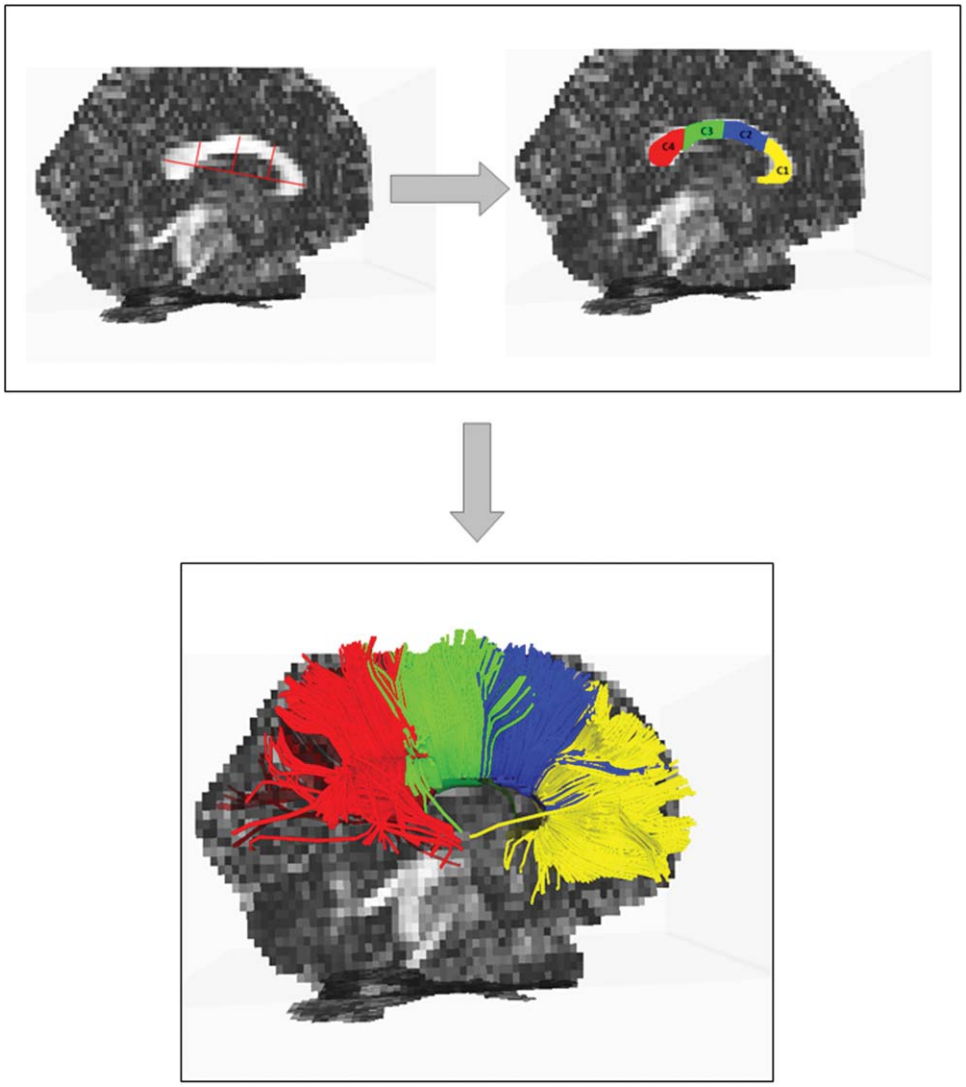

Figure 1. Corpus callosum fiber tracts. Upper left: Regions of interest in a mid-sagittal section of the GFA map in native space. Red lines indicate the anterior–posterior extension of the corpus callosum and the perpendicular sections to define corpus callosum subregions. Upper right: C1 to C4 indicate the corpus callosum subregions in anterior to posterior direction. Lower row: Fiber tracts originating from the corpus callosum subregions C1 to C4 determined using DSI Studio.

seed region in a coronal view lateral to the cerebellar peduncles and a pass region inferior to the corpus callosum splenium. Seed regions and pass regions had a diameter between 10 mm and 11 mm, depending on the size of the respective structure in the individual brain scan. Only tracts with an angle $<30^{\circ}$ and a fiber length between 20 and 60 mm were allowed.

For each reconstructed fiber tract, we determined the average GFA along the tract.

Voxel-Based Analysis

For voxel-based analysis we reconstructed GFA maps using DSI Studio. Each GFA map in native space was rigidly coregistered with the corresponding structural MRI scan. The co-registered GFA maps were then warped into MNI space using the flow-fields resulting from the DARTEL registration of the GM and WM maps to the IXI-template. Voxel values of warped GFA maps were not modulated to exclude effects of local atrophy in the GFA maps. Estimates from rigid co-registration and nonlinear warping were combined into one transformation to avoid separate interpolation steps. Warped GFA maps were resliced to an isotropic voxel-size of 1.5 mm^3, masked using a binarized WM mask averaged across the 35 subjects to exclude voxels outside the cerebral WM from subsequent analysis, and smoothed with a Gaussian smoothing kernel of 8 mm FWHM.

Statistical Analysis

Voxel Based Analysis

For the voxel-based analysis we used the general linear model within the SPM framework. We determined effects of age on the smoothed GM, WM, and GFA maps. Results were thresholded at $P < 0.05$, false discovery rate (FDR) corrected for multiple comparisons with a minimum cluster extension threshold of 50 contiguous voxels (corresponding to a volume of 168.75 mm^3). Effects were anatomically localized for DSI data according to the JHU White Matter Tractography Atlas (35), for GM volume according to the automated anatomical labeling (AAL) atlas (36).

Tract-based Analysis

We used separate linear models to regress age and squared age on GFA in each of the fiber tracts, the

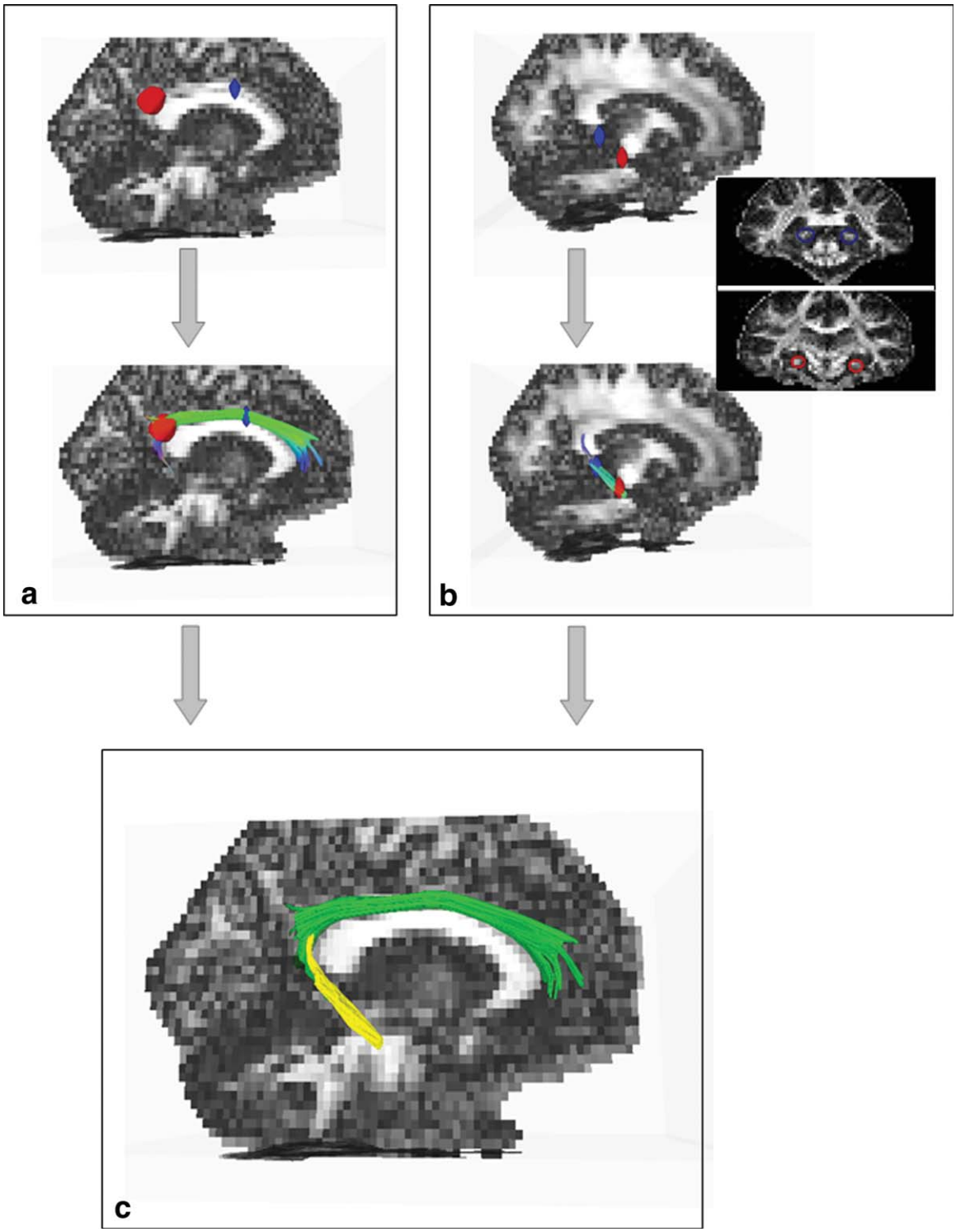

Figure 2. Superior and inferior cingulum bundle. Localizations of seed regions (red) and pass regions (blue) to determine cingulum fiber tracts. **a:** Placing of the seed region superior to the splenium of the corpus callosum and of the pass region superior to the middle truncus of the corpus callosum (upper half) and resulting superior cingulum bundle (lower half). **b:** Placing of the seed region superior lateral to the cerebellar peduncles and of the pass region inferior to the splenium of the corpus callosum (upper half) and resulting inferior cingulum bundle (lower half). The right hand side depicts the placing of the seed and pass regions in coronal sections. **c:** Superior and inferior cingulum fiber tracts combined.

GM volume of the significant GM clusters from voxel-based analysis, as well as total GM, WM, and intracranial volumes. Significant effects were followed-up by multiple linear regressions controlling for gender, ApoE4 genotype, the interaction between age and ApoE4 genotype and the VLMT global learning score. Associations between age and VLMT performance, and VLMT performance and GFA values in fiber tracts were assessed using bivariate linear regression. The level of significance was set at $P < 0.05$.

Inter-rater reliability was determined from 10 randomly selected data sets that had been traced by two independent raters, using the intraclass correlation coefficient.

RESULTS

Subjects' Characteristics

Subjects were matched for gender across ages. Years of education were not different across different ages ($F^5_{170} = 1.3$; $P = 0.28$) and were not different between women and men ($T_{33} = 0.03$; $P = 0.98$), with a mean value of 14.7 years (SD 1.9), ranging between 12 and 18 years. Although not matched a priori, ApoE4 genotype was homogeneously distributed across ages ($\chi^2 = 4.9$; $P = 0.42$), with 23 subjects without an ApoE4 allele, 11 subjects with one ApoE4 allele and one subject with two ApoE4 alleles. When assessing the association between age and VLMT performance, only the global learning score was significantly correlated with age ($r_{35} = -0.41$, $P < 0.014$).

DSI Data

The inter-rater reliability, using the intraclass correlation coefficient, for mean GFA of reconstructed fiber tracts originating from the corpus callosum ranged between 0.954 and 0.996 across corpus callosum subregions. For the cingulum bundle, inter-rater reliability was 0.965 and 0.933 for left and right superior cingulum bundle, respectively, and 0.765 and 0.824 for left and right inferior cingulum bundle, respectively.

We found a significant effect in a quadratic model for age on the GFA of fiber tracts originating from the anterior corpus callosum subregions C1 ($R^2 = 0.39$; $P < 0.001$) and C2 ($R^2 = 0.12$; $P < 0.05$) (Fig. 3). There was no significant contribution of a linear term in either model. The GFA of tracts originating from corpus callosum subregions other than C1 or C2 and the entire corpus callosum showed no significant association with age. The effect of squared age on C1 and C2 was preserved after accounting for gender, ApoE4 genotype, the interaction between squared age and ApoE4 genotype and the VLMT global learning score. There was no significant correlation of age with mean GFA of superior or inferior cingulum fibers.

Volumes of tracts were not significantly different across ages with exception of the most posterior corpus callosum region that showed a reduced tract volume with increasing age ($F^5_{170} = 3.02$; $P < 0.05$).

When we calculated FA values from the DSI data set according to Jiang et al (37), effects of age on corpus callosum FA were similar to effects on GFA with a quadratic model for age significantly correlating with the FA of fiber tracts originating from the anterior corpus callosum subregions C1 ($R^2 = 0.36$; $P < 0.001$) and C2 ($R^2 = 0.24$; $P < 0.03$). Using, however, our seed and pass regions we could not derive reliable fiber tracts for inferior and superior cingulate bundle from the DTI data reconstruction.

ApoE4 genotype was significantly correlated with GFA in fiber tracts originating from C2 ($r_{35} = 0.42$; $P < 0.02$) and C3 ($r_{35} = 0.41$; $P < 0.02$), indicating higher GFA in ApoE4 carriers, but not with other corpus callosum subregions. The effect of ApoE4 genotpye on GFA in C2 and C3 was preserved after accounting for age and gender. Years of education were associated with GFA in left superior cingulum bundle ($r = 0.49$; $P < 0.003$), but not with any other fiber tract. The effect of years of education on GFA in left cingulum bundle was preserved after accounting for age, gender, and global learning score in the VLMT. There were no significant correlations of VLMT performance measures and gender with the GFA in corpus callosum and cingulum fiber tracts.

Results of the voxel-based analysis are summarized in Table 1 and Figure 4. We found significant decline of GFA with age at $P < 0.05$, FDR corrected, in widespread areas involving anterior corpus callosum, fornix, pyramidal tract, and areas projecting on anterior thalamic radiation, inferior longitudinal fasciculus, superior longitudinal fasciculus, and inferior frontooccipital fasciculus.

Anatomical Data

We found significant decline of total cerebral GM volume with age ($r = -0.59$, $P < 0.0001$), but no effect of age on total WM volume ($r = 0.08$; $P = 0.64$) or total intracranial volume ($r = 0.001$; $P = 0.99$). The two most anterior corpus callosum cross-sectional areas (genu and anterior truncus) were significantly correlated with age ($r = -0.37$ and $r = -0.39$, respectively; both $P < 0.05$). This effect was accounted for by the effect of age on anterior corpus callosum GFA in partial regression analysis (C1 area: partial $r = -0.25$; $P = 0.16$, controlling for C1 GFA, and C2 area: partial $r = -0.31$; $P = 0.08$, controlling for C2 GFA), whereas the effect of age on anterior corpus callosum GFA was preserved after accounting for anterior corpus callosum area (C1 GFA: partial $r = -0.56$; $P < 0.001$, controlling for C1 area). Total corpus callosum cross-sectional area and the remaining corpus callosum subregions were not correlated with age ($P > 0.17$ for all comparisons). All results remained essentially unchanged when using a quadratic term of age for correlation analysis.

Using voxel-based analysis, we found significant decline of GM volume with age in bilateral superior temporal gyrus and inferior frontal gyrus (Table 2 and Fig. 5). A square function of age had a significant effect on the GM density extracted from the significant clusters ($R^2 = 0.73$; $P < 0.0001$) (Fig. 6). There was no significant additional contribution of a linear term of age.

Voxel-based analysis of WM volume revealed no significant cluster at an FDR corrected level of significance of $P < 0.05$.

DISCUSSION

We applied DSI to study effects of age on subcortical fiber tract integrity across the adult life span in a group of 35 cognitively healthy subjects. We focused

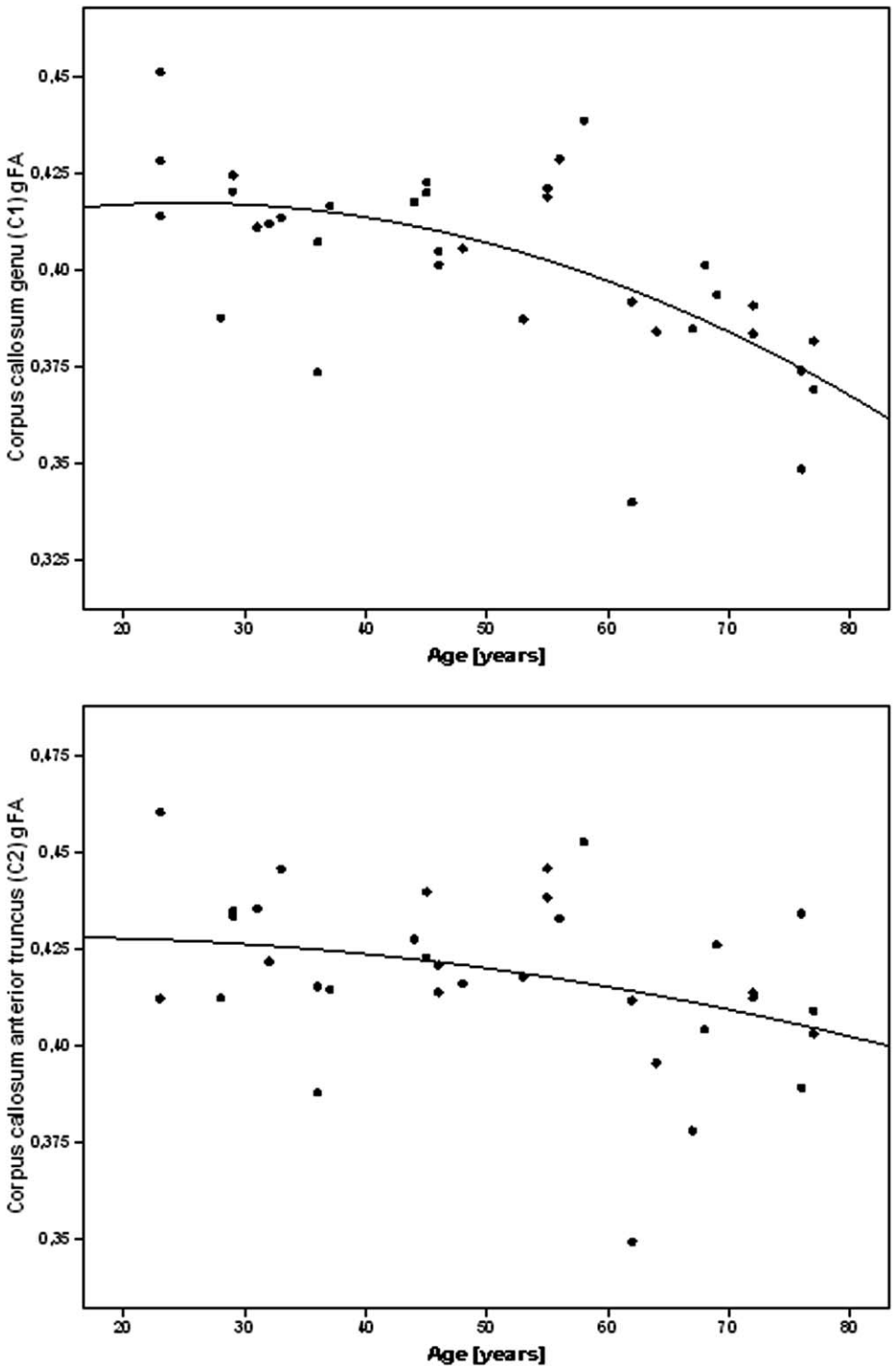

Figure 3. Decline of GFA in anterior corpus callosum subregions with age. Scatter plot of age versus GFA in the fiber tracts originating from the C1 (top) and C2 (bottom) subregions. The black line indicates the second order polynomial regression line.

on fiber tracts originating from the corpus callosum and the cingulum bundle to replicate and extend earlier findings using DTI. We found a significant decline of anterior corpus callosum fiber tract integrity over the adult life span. Complementary voxel-based analysis showed significant decline of GFA predominantly in frontal lobe WM areas. In contrast, GM volume reductions were more pronounced in lateral temporal cortex. Effect of age on WM volume was limited to anterior corpus callosum and was mediated by the effect of age on GFA. Consistent with previous studies (38), total learning in the VLMT declined with age. However, no other VLMT index was affected by age in our sample, supporting the notion that elderly participants in this study were cognitively healthy. The reliability of our fiber tractography was very high in corpus callosum and superior cingulum bundle. Measurement of inferior cingulum bundle was less reliable, possibly due to the difficulties of the algorithm to find consistent tracks in this brain area. We had tried different reconstruction algorithms, but results were less consistent than those for the other regions.

Table 1
Clusters of Significant GFA Decline With Age*

No. of voxels	COG_x	COG_y	COG_z	Prob.	Fiber tracts 1	Prob.	Fiber tracts 2
9619	21	31	7	63%	Anterior thalamic radiation R	18%	Inferior fronto-occipital fasciculus R
7386	−20	31	8	24%	Anterior thalamic radiation L	16%	Forceps minor
2180	32	−67	−3	32%	Inferior longitudinal fasciculus R	16%	Inferior fronto-occipital fasciculus R
2073	−24	−62	−43	3%	Corticospinal tract L	3%	Anterior thalamic radiation L
1470	36	−55	22	5%	Superior longitudinal fasciculus R	3%	Inferior longitudinal fasciculus R
1004	−34	−67	14	8%	Inferior longitudinal fasciculus L	8%	Inferior fronto-occipital fasciculus L
893	−35	7	17	11%	Superior longitudinal fasciculus L	8%	Superior longitudinal fasciculus L
522	25	−28	−3	3%	Inferior fronto-occipital fasciculus		
512	1	−8	14	80%	Fornix		
470	−45	−30	−5	13%	Inferior longitudinal fasciculus L		
375	44	−32	−3	5%	Inferior longitudinal fasciculus R		
251	20	−14	39	3%	Corticospinal tract R		

*The height threshold was set at $P < 0.05$, FDR corrected. The cluster extension representing the number of contiguous voxels passing the height threshold was set at $k > 50$. Centers of gravity of the clusters ($COG_{x,y,z}$) are indicated by MNI coordinates x, y, and z: x = the medial to lateral distance relative to midline (positive = right hemisphere); y = the anterior to posterior distance relative to the anterior commissure (positive = anterior); z = superior to inferior distance relative to the anterior commissure -posterior commissure line (positive = superior). Prob. is the probability of the cluster to belong to the respective fiber tract derived from the JHU White Matter Tractography Atlas (35).
R/L = right/left.

Despite the general preservation of cognitive function, in the elderly subjects GFA was significantly reduced in anterior corpus callosum fibers in the tract-based analysis. These findings were confirmed and extended by the voxel-based analysis showing anterior corpus callosum changes together with a decline of GFA in anterior portions of the superior and inferior longitudinal fasciculus and the anterior thalamic radiation. Predominant decline of anterior corpus callosum fiber tract integrity agrees with previous studies using conventional DTI (39). The effect of age was nonlinear and agrees with previous studies on volumetric and fiber tract integrity measures (40,41), suggesting a relative preservation of fiber tract integrity up to middle age with an accelerated decline thereafter. A previous study has suggested using smoothing splines or higher order polynomial functions rather than quadratic functions to determine the age at which the effects of aging accelerate, because quadratic functions are sensitive to the selection of the sampled age range (42). The size of our sample is not sufficient to estimate a stable smoothing spline or higher order polynomial function. Our data confirm that the effect of age on fiber tract integrity as measured by DSI is significantly nonlinear, however, we cannot provide an unbiased estimate of the age at which the decline of fiber tract integrity starts to accelerate. The decline of GFA mediated the effect of age on anterior corpus callosum area. This finding is consistent with evidence from human and nonhuman primate studies on the substantial loss of myelinated fibers in corpus callosum and other brain areas with normal aging (43–45).

The relative preservation of fiber tract integrity in cingulum bundle with age in our cognitively healthy subjects agrees with previous findings comparing cognitively stable and cognitively declining subjects where smaller mean diffusivity (as indicator of preserved fiber tract integrity) was associated with preserved cognitive function (46).

When we reconstructed our diffusion data according to a DTI scheme (37), reductions with age in anterior corpus callosum subregions were similar for fractional anisotropy (FA) compared with GFA. However, using our seed and pass regions we could not reconstruct reliable fiber tracts for inferior and superior cingulated bundle from the DTI data, consistent with the notion that DSI data may be superior to DTI data to reconstruct complex fiber tracts (11). These findings suggest that for tracts with one predominant fiber direction such as the corpus callosum, DSI data may bear little advantage over classical DTI data. However, with more complex tracts, fiber tracking appears to be more reliable using DSI than DTI data.

In our sample, GM volume reductions were most pronounced in the lateral temporal lobe areas, planum temporale, and insula, and to a lesser extent in the prefrontal cortex and cerebellum. This agrees partly with findings in a large cohort of 465 subjects, where effects of age on cortical GM volume were most pronounced in the superior parietal gyri, insula, planum temporale, postcentral gyrus, and middle frontal gyrus as well as the posterior cerebellum (47). Effects in our cohort were more pronounced in lateral temporal cortex than in the previous study and less pronounced in anterior cingulate and superior parietal cortex. We had a much smaller group of subjects compared with the previous study, reducing the power in our sample to detect similarily wide-spread effects of aging. Similar to the previous study, however, hippocampus, entorhinal cortex, and subcortical nuclei were largely spared by the effects of aging.

The fiber tracts that showed significant age-related decline in microstructural integrity partly correspond with the cortical areas affected by aging. Thus, the anterior corpus callosum has been shown to project toward prefrontal and lateral temporal cortex, whereas anterior temporal cortex is connected by means of the anterior commissure and parietal cortex

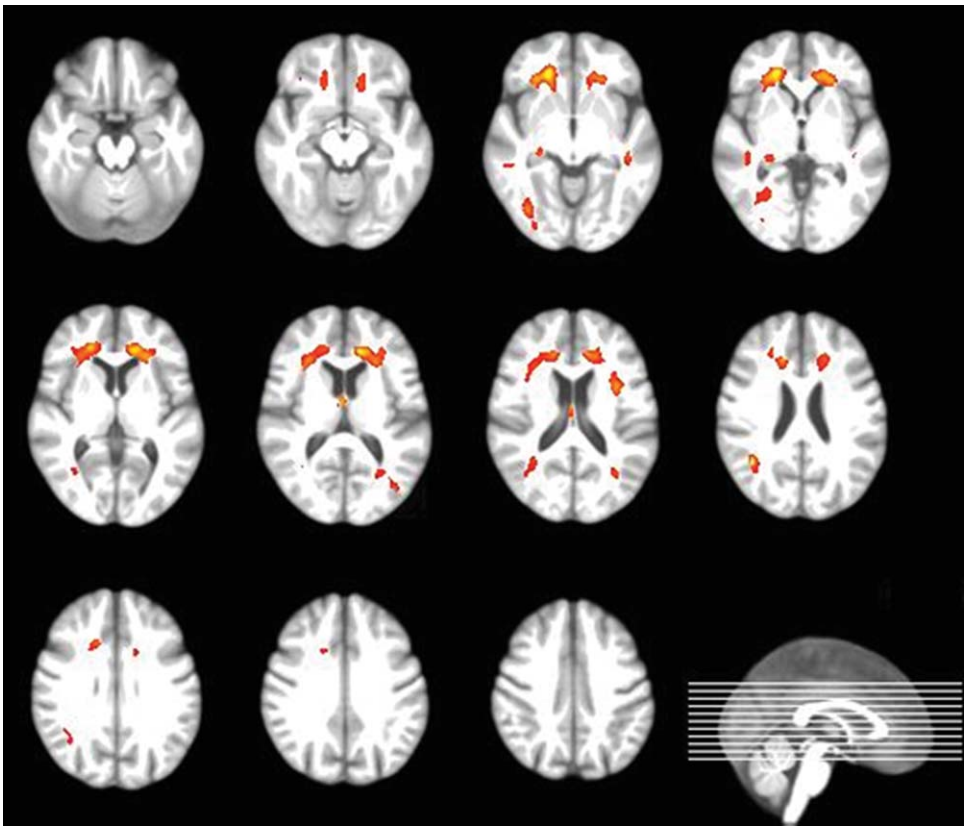

Figure 4. Voxel-based changes in GFA. Areas of significant decline of GFA with age (at least 50 contiguous voxels with $P < 0.05$, FDR corrected) in red projected on transversal sections of the averaged brain from all subjects in MNI space. The height of the transversal sections is indicated on a sagittal section though the averaged brain in the lower right corner.

mainly through the posterior part of the corpus callosum body and the splenium (48). The superior longitudinal fasciculus connects prefrontal with superior parietal and lateral temporal lobe areas. The involvement of the corticospinal tract agrees with the age effect on the precentral cortex. Inferior longitudinal fasciculus connects lateral temporal with occipital brain areas, including lingual and fusiform gyrus. Based on the anterior to posterior gradient in age effects on subcortical fiber tract integrity one can speculate that the relatively stronger involvement of lateral temporal, inferior parietal and occipital GM results from the disconnection of severed long reaching fiber bundles such as the inferior and superior longitudinal fasciculi. This interpretation agrees with a recent study in a large number of healthy subjects using conventional DTI and cortical thickness measurement, suggesting that changes in FA account for changes in cortical thickness over the adult age range, possibly reflecting underlying changes in myelination (49).

GFA reductions occurred in the absence of global or regional changes in WM volume in the voxel-based analysis and mediated the effect of age on corpus callosum area. This indicates that GFA measurements are more sensitive for age effects than commonly used

Table 2
Significant Decline of Gray Matter Volume With Age

x	y	z	T_{34}	Side	Prob.	Area I	Prob.	Area II
42	20	−6	6.56	R	82%	Insula	10%	Frontal orbital inferior
46	−12	6	6.17	R	38%	Superior temporal gyrus	24%	Heschl gyrus
−45	−3	−3	5.89	L	66%	Superior temporal gyrus	19%	Heschl gyrus
10	−36	0	5.44	R	27%	Lingual gyrus	20%	Thalamus
−52	17	4	5.43	L	100%	Inferior frontal gyrus		
−51	−13	33	5.08	L	89%	Postcentral gyrus	11%	Precentral gyrus
60	−49	13	5.07	R	75%	Middle temporal gyrus	25%	Superior temporal gyrus
58	−64	7	5.03	R	100%	Middle temporal gyrus		
26	−79	−9	4.55	R	73%	Fusiform gyrus	27%	Lingual gyrus
−38	−48	−30	4.47	L	64%	Cerebellum	36%	Crus cerebelli

* The height threshold was set at $P < 0.05$, FDR corrected. The cluster extension representing the number of contiguous voxels passing the height threshold was set at $k > 50$. Brain regions are indicated by MNI coordinates x, y, and z: x = the medial to lateral distance relative to midline (positive = right hemisphere); y = the anterior to posterior distance relative to the anterior commissure (positive = anterior); z = superior to inferior distance relative to the anterior commissure -posterior commissure line (positive = superior). Prob. is the probability of the cluster to belong to the respective anatomical region derived from the automated anatomical labeling (AAL) atlas (36).
R/L = right/left.

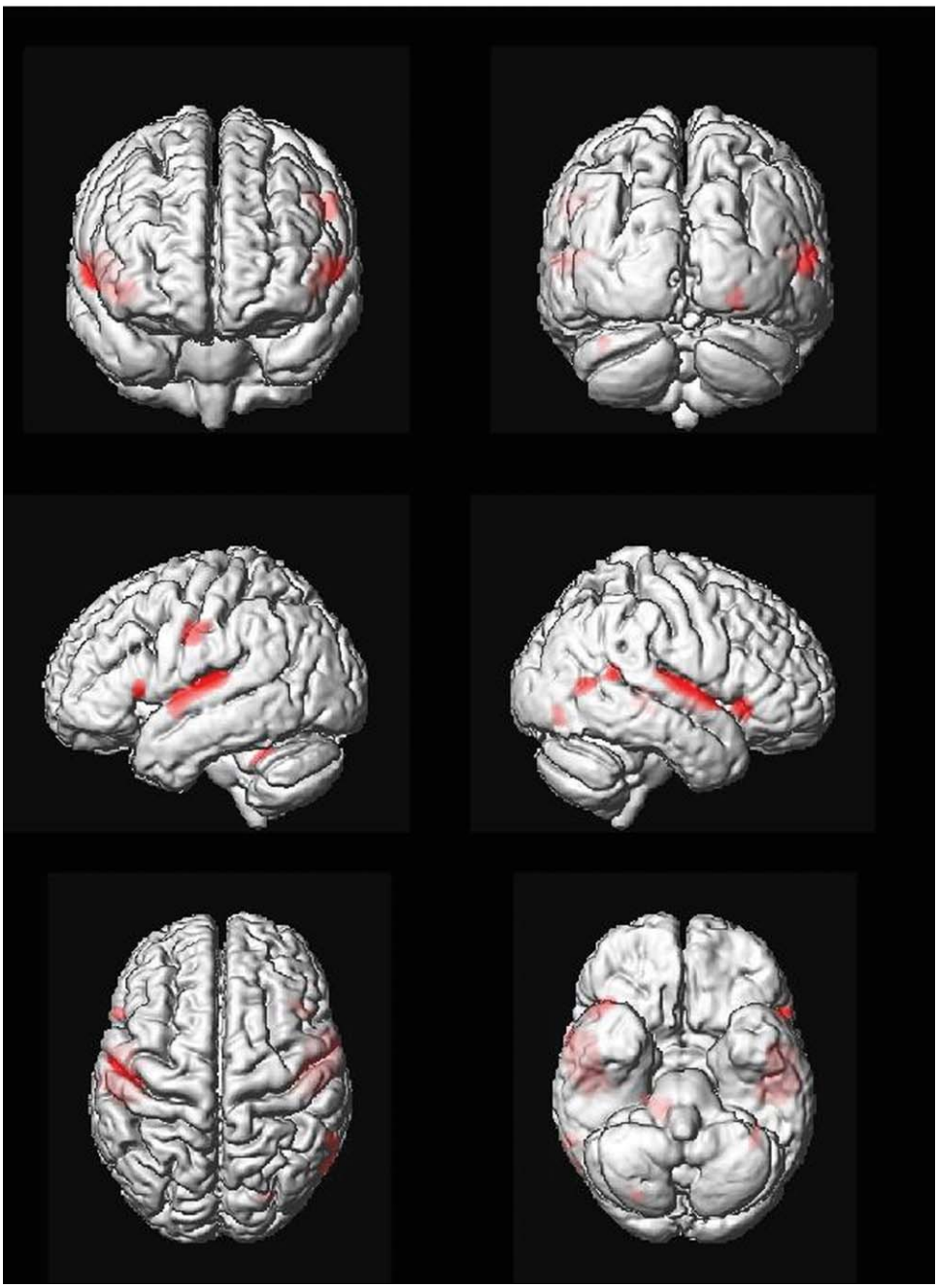

Figure 5. Voxel-based changes in GM volume with age. Areas of significant decline of GM volume with age (at least 50 contiguous voxels with $P < 0.05$, FDR corrected) in red projected on the rendered surface of the averaged brain from all subjects in MNI space.

volumetric measures, and that microstructural alterations of subcortical WM may precede loss of WM tissue volume. In addition, mechanisms of gliosis and axonal swelling may mask volumetric WM effects of aging.

Effects of ApoE4 genotype, a genetic risk factor for sporadic Alzheimer's disease (50), were very limited. Only the anterior corpus callosum, the area that was also most strongly affected by age, showed a larger GFA in subjects with at least one ApoE4 risk allele, even after accounting for the effect of age. This seems counter-intuitive as one might expect that a risk factor for AD would lead to early damage to cerebral structural integrity. On the contrary, a recent study in healthy elderly subjects showed larger volume of hippocampus in cognitively healthy elderly subjects with cortical amyloid deposition compared with age-matched subjects without amyloid deposition (51). As amyloid-deposition is a major risk factor for the manifestation of Alzheimer's disease, the increased hippocampus volume was interpreted as indicating a factor of resilience, partly accounting for the fact that subjects with significant amyloid load were still cognitively unimpaired. The higher integrity of anterior corpus callosum fiber tracts with ApoE4 genotype may represent a similar mechanism. It may indicate a trait marker of resilience that supports the preservation of cognitive performance in the presence of a genetic risk marker of Alzheimer's disease.

One has to keep in mind that the cross-sectional nature of our data allows no direct inference on the effect of aging on brain structure and cognitive

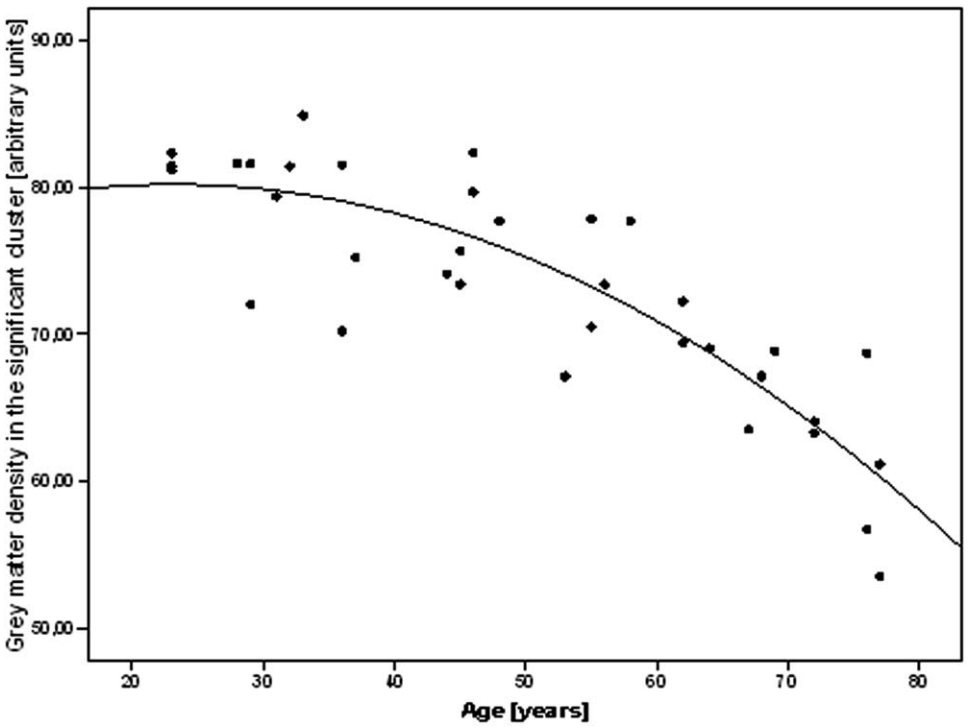

Figure 6. Decline of GM volume with age. Scatter plot of age versus signal intensity over all GM clusters that were significantly associated with age in the voxel-based analysis. The black line indicates the second order polynomial regression line.

performance. Cross-sectional studies on different age cohorts can easily be affected by secular effects for example on body height and on the level of educational achievement accessible to women several decades ago. However, longitudinal studies that would avoid these problems are impractical over this wide age range. Effects of body height have been amended by modulating volumes only for nonlinear effects thus taking into account linear effects of overall brain size. In addition, total intracranial volume was not different across age cohorts. Accounting for a secular effect on education, we had selected a cognitively healthy cohort of elderly subjects with a higher than average level of education for their age group. Therefore, there was no difference in years of education across age cohorts and between sexes. However, we may even have introduced a secular bias in the opposite direction by including elderly subjects with higher than average cognitive reserve. Because higher education has been shown to be associated with preserved WM integrity in cognitively normal elderly subjects (52), these selection criteria would lead to a conservative estimate of age-related changes in the present study.

In conclusion, our data derived from a novel DSI acquisition suggest a significant nonlinear decline of fiber tract integrity with aging even in absence of significant cognitive decline in a cognitively healthy group of subjects, replicating and extending previous findings from conventional DTI. If replicated in future studies, DSI may become a useful marker for WM degeneration in healthy and pathological aging, particularly in areas with complex fiber structure, such as the cingulum bundle. Subsequent studies will focus on age-related changes of selective fiber tracts underlying functionally connected brain areas in resting state networks. In addition, given the potential of DSI to resolve crossing fibers in complex intracortical projecting fiber tracts the future use of DSI may increase accuracy of fiber tracking in neuropsychiatric diseases, such as arcuate fasciculus in primary progressive aphasia, anterior cingulate in schizophrenia, or cingulum bundle in Alzheimer's disease, and provide access to fiber tracts that cannot reliably be tracked using DTI, such as projections from the cholinergic basal forebrain nuclei.

ACKNOWLEDGMENTS

We thank the staff of the Department of Radiology, University of Rostock, for technical support. We thank Siemens Medical Solutions, Erlangen, Germany, for providing the WIP #603 sequence. Part of this work was supported by grants from the Interdisciplinary Faculty, Department "Ageing of the Individual and the Society", University of Rostock, to S.J.T. and of the Hirnliga e. V. (Nürmbrecht, Germany) to S.J.T.

REFERENCES

1. DeCarli C, Massaro J, Harvey D, et al. Measures of brain morphology and infarction in the framingham heart study: establishing what is normal. Neurobiol Aging 2005;26:491–510.
2. Jernigan TL, Archibald SL, Fennema-Notestine C, et al. Effects of age on tissues and regions of the cerebrum and cerebellum. Neurobiol Aging 2001;22:581–594.
3. Freeman SH, Kandel R, Cruz L, et al. Preservation of neuronal number despite age-related cortical brain atrophy in elderly subjects without Alzheimer disease. J Neuropathol Exp Neurol 2008; 67:1205–1212.
4. Makris N, Worth AJ, Sorensen AG, et al. Morphometry of in vivo human white matter association pathways with diffusion-weighted magnetic resonance imaging. Ann Neurol 1997;42: 951–962.

5. Basser PJ, Pierpaoli C. Microstructural and physiological features of tissues elucidated by quantitative-diffusion-tensor MRI. J Magn Reson B 1996;111:209–219.
6. Beaulieu C, Allen PS. Determinants of anisotropic water diffusion in nerves. Magn Reson Med 1994;31:394–400.
7. Sullivan EV, Pfefferbaum A. Diffusion tensor imaging and aging. Neurosci Biobehav Rev 2006;30:749–761.
8. Stadlbauer A, Ganslandt O, Salomonowitz E, et al. Magnetic resonance fiber density mapping of age-related white matter changes. Eur J Radiol 2012;81:4005–4012.
9. Teipel SJ, Meindl T, Wagner M, et al. Longitudinal changes in fiber tract integrity in healthy aging and mild cognitive impairment: a DTI follow-up study. J Alzheimers Dis 2010;22:507–522.
10. Wiegell MR, Larsson HB, Wedeen VJ. Fiber crossing in human brain depicted with diffusion tensor MR imaging. Radiology 2000; 217:897–903.
11. Wedeen VJ, Wang RP, Schmahmann JD, et al. Diffusion spectrum magnetic resonance imaging (DSI) tractography of crossing fibers. Neuroimage 2008;41:1267–1277.
12. Hagmann P, Jonasson L, Deffieux T, Meuli R, Thiran JP, Wedeen VJ. Fibertract segmentation in position orientation space from high angular resolution diffusion MRI. Neuroimage 2006;32:665–675.
13. Nezamzadeh M, Wedeen VJ, Wang R, et al. In-vivo investigation of the human cingulum bundle using the optimization of MR diffusion spectrum imaging. Eur J Radiol 2010;75:e29–e36.
14. Sullivan EV, Rohlfing T, Pfefferbaum A. Longitudinal study of callosal microstructure in the normal adult aging brain using quantitative DTI fiber tracking. Dev Neuropsychol 2010;35:233–256.
15. Shu N, Wang Z, Qi Z, Li K, He Y. Multiple diffusion indices reveals white matter degeneration in Alzheimer's disease and mild cognitive impairment: a tract-based spatial statistics study. J Alzheimers Dis 2011;26(Suppl 3):275–285.
16. Teipel SJ, Bokde AL, Meindl T, et al. White matter microstructure underlying default mode network connectivity in the human brain. Neuroimage 2010;49:2021–2032.
17. O'Dwyer L, Lamberton F, Matura S, et al. Reduced hippocampal volume in healthy young ApoE4 carriers: an MRI study. PloS One 2012;7:e48895.
18. Kljajevic V, Meyer P, Holzmann C, et al. The ϵ4 genotype of Apolipoprotein E and white matter integrity in Alzheimer's disease. Alzheimers Dementia 2013 [Epub ahead of print].
19. Hardy J. ApoE, amyloid, and Alzheimer's disease. Science 1994; 263:454–455.
20. Tuch DS, Reese TG, Wiegell MR, Wedeen VJ. Diffusion MRI of complex neural architecture. Neuron 2003;40:885–895.
21. Nasreddine ZS, Phillips NA, Bedirian V, et al. The Montreal Cognitive Assessment, MoCA: a brief screening tool for mild cognitive impairment. J Am Geriatr Soc 2005;53:695–699.
22. Morris JC, Heyman A, Mohs RC, et al. The Consortium to Establish a Registry for Alzheimer's Disease (CERAD). Part I. Clinical and neuropsychological assessment of Alzheimer's disease. Neurology 1989;39:1159–1165.
23. Chen P, Ratcliff G, Belle SH, Cauley JA, DeKosky ST, Ganguli M. Cognitive tests that best discriminate between presymptomatic AD and those who remain nondemented. Neurology 2000;55: 1847–1853.
24. Shulman KI, Shedletsky R, Silver IL. The challenge of time: clock drawing and cognitive function in the elderly. Int J Geriatr Psychiatry 1986;1:135–140.
25. Folstein MF, Folstein SE, McHugh PR. Mini-mental-state: a practical method for grading the cognitive state of patients for the clinician. J Psychiatr Res 1975;12:189–198.
26. Morris JC. The Clinical Dementia Rating (CDR): current version and scoring rules. Neurology 1993;43:2412–2414.
27. Spitzer RL, Kroenke K, Williams JB. Validation and utility of a self-report version of PRIME-MD: the PHQ primary care study. Primary care evaluation of mental disorders. Patient health questionnaire. JAMA 1999;282:1737–1744.
28. Helmstaedter C, Durwen HF. [The Verbal Learning and Retention Test. A useful and differentiated tool in evaluating verbal memory performance]. Schweiz Arch Neurol Psychiatr 1990;141:21–30.
29. Rosenberg SJ, Ryan JJ, Prifitera A. Rey Auditory-Verbal Learning Test performance of patients with and without memory impairment. J Clin Psychol 1984;40:785–787.
30. Vakil E, Greenstein Y, Blachstein H. Normative data for composite scores for children and adults derived from the Rey Auditory Verbal Learning Test. Clin Neuropsychol 2010;24:662–677.
31. Reese TG, Heid O, Weisskoff RM, Wedeen VJ. Reduction of eddy-current-induced distortion in diffusion MRI using a twice-refocused spin echo. Magn Reson Med 2003;49:177–182.
32. Ashburner J. A fast diffeomorphic image registration algorithm. Neuroimage 2007;38:95–113.
33. Hampel H, Teipel SJ, Alexander GE, et al. Corpus callosum atrophy is a possible indicator of region- and cell type-specific neuronal degeneration in Alzheimer disease: a magnetic resonance imaging analysis. Arch Neurol 1998;55:193–198.
34. Yeh F-C, Wedeen VJ, Tseng W-YI. Generalized Q-sampling imaging. IEEE transactions on medical imaging 2010;27:1415–1424.
35. Wakana S, Jiang H, Nagae-Poetscher LM, van Zijl PC, Mori S. Fiber tract-based atlas of human white matter anatomy. Radiology 2004;230:77–87.
36. Tzourio-Mazoyer N, Landeau B, Papathanassiou D, et al. Automated anatomical labeling of activations in SPM using a macroscopic anatomical parcellation of the MNI MRI single-subject brain. Neuroimage 2002;15:273–289.
37. Jiang H, van Zijl PC, Kim J, Pearlson GD, Mori S. DtiStudio: resource program for diffusion tensor computation and fiber bundle tracking. Comput Methods Programs Biomed 2006;81:106–116.
38. Blachstein H, Greenstein Y, Vakil E. Aging and temporal order memory: a comparison of direct and indirect measures. J Clin Exp Neuropsychol 2012;34:107–112.
39. Sullivan EV, Adalsteinsson E, Pfefferbaum A. Selective age-related degradation of anterior callosal fiber bundles quantified in vivo with fiber tracking. Cereb Cortex 2006;16:1030–1039.
40. Kennedy KM, Raz N. Aging white matter and cognition: differential effects of regional variations in diffusion properties on memory, executive functions, and speed. Neuropsychologia 2009;47: 916–927.
41. Walhovd KB, Westlye LT, Amlien I, et al. Consistent neuroanatomical age-related volume differences across multiple samples. Neurobiol Aging 2011;32:916–932.
42. Fjell AM, Walhovd KB, Westlye LT, et al. When does brain aging accelerate? Dangers of quadratic fits in cross-sectional studies. Neuroimage 2010;50:1376–1383.
43. Bowley MP, Cabral H, Rosene DL, Peters A. Age changes in myelinated nerve fibers of the cingulate bundle and corpus callosum in the rhesus monkey. J Comp Neurol 2010;518:3046–3064.
44. Marner L, Nyengaard JR, Tang Y, Pakkenberg B. Marked loss of myelinated nerve fibers in the human brain with age. J Comp Neurol 2003;462:144–152.
45. Meier-Ruge W, Ulrich J, Bruhlmann M, Meier E. Age-related white matter atrophy in the human brain. Ann N Y Acad Sci 1992;673:260–269.
46. Rosano C, Aizenstein HJ, Newman AB, et al. Neuroimaging differences between older adults with maintained versus declining cognition over a 10-year period. Neuroimage 2012;62:307–313.
47. Good CD, Johnsrude IS, Ashburner J, Henson RN, Friston KJ, Frackowiak RS. A voxel-based morphometric study of ageing in 465 normal adult human brains. NeuroImage 2001;14(Pt 1):21–36.
48. De Lacoste MC, Kirkpatrick JB, Ross ED. Topography of the human corpus callosum. J Neuropathol Exp Neurol 1985;44: 578–591.
49. Kochunov P, Glahn DC, Lancaster J, et al. Fractional anisotropy of cerebral white matter and thickness of cortical gray matter across the lifespan. Neuroimage 2011;58:41–49.
50. Coon KD, Myers AJ, Craig DW, et al. A high-density whole-genome association study reveals that APOE is the major susceptibility gene for sporadic late-onset Alzheimer's disease. J Clin Psychiatry 2007;68:613–618.
51. Chetelat G, Villemagne VL, Pike KE, et al. Larger temporal volume in elderly with high versus low beta-amyloid deposition. Brain 2010;133:3349–3358.
52. Teipel SJ, Meindl T, Wagner M, et al. White matter microstructure in relation to education in aging and Alzheimer's disease. J Alzheimers Dis 2009;17:571–583.